THE JOURNAL OF PHYSICAL CHEMISTRY Letters

Letter

pubs.acs.org/JPCL

Identification of Possible Pathways for C−C Bond Formation during Electrochemical Reduction of CO_2: New Theoretical Insights from an Improved Electrochemical Model

Jason D. Goodpaster,[†] Alexis T. Bell,[*,‡] and Martin Head-Gordon[*,§]

[†]The Joint Center for Artificial Photosynthesis, Lawrence Berkeley National Laboratory, Berkeley, California 94720, United States

[‡]Department of Chemical and Biomolecular Engineering, University of California at Berkeley, Berkeley, California 94720, United States

[§]Department of Chemistry, University of California at Berkeley, Berkeley, California 94720, United States

Supporting Information

ABSTRACT: We have carried out a periodic Kohn−Sham density functional theory investigation of the pathways by which carbon−carbon bonds could be formed during the electrochemical reduction of CO_2 on Cu(100) using a model that includes the effects of the electrochemical potential, solvent, and electrolyte. The electrochemical potential was set by relating the applied potential to the Fermi energy and then calculating the number of electrons required by the simulation cell for that specific Fermi energy. The solvent was included as a continuum dielectric, and the electrolyte was described using a linearized Poisson−Boltzmann model. The calculated potential of zero charge for a variety of surfaces agrees with experiment to within a mean average error of 0.09 V, thereby validating the assumptions of the model. Analysis of the mechanism for C−C bond formation revealed that at low-applied potential, C−C bond formation occurs through a CO dimer. However, at high applied potentials, a large activation barrier blocks this pathway; therefore, C−C bond formation occurs through reaction of adsorbed CHO and CO. Rate parameters determined from our calculations were used to simulate the kinetics of ethene formation during the electrochemical reduction of CO over a Cu(100) surface. An excellent match was observed between previously reported measurements of the partial current for ethene formation as a function of applied voltage and the variation in the partial current for C−C bond formation predicted by our microkinetic model. The electrochemical model reported here is simple, fairly easy to implement, and involves only a small increase in computational cost over calculations neglecting the effects of the electrolyte and the applied field. Therefore, it can be used to study the effects of applied potential and electrolyte composition on the energetics of surface reactions for a wide variety of electrochemical reactions.

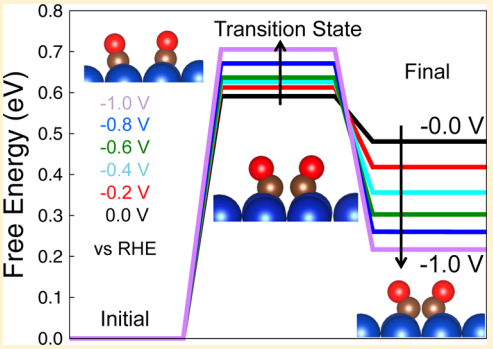

The reduction of CO_2 to fuels provides a promising pathway to a carbon-neutral energy cycle. Despite extensive effort in recent years, the development of a practical process has been hindered by the high overpotentials and low selectivity of available catalysts.[1] Copper electrodes have been shown to produce primarily methane and ethene, but the mechanism by which these products are formed remains a subject of ongoing discussion.[2] In particular, the mechanism for carbon−carbon bond formation and the influence of the applied potential on the rate of this step have remained elusive.[2−6] Recent experiments by Koper and co-workers have suggested that ethene formation proceeds through different pathways at low versus high applied potentials.[7−10] Koper and co-workers and Hori and co-workers have also shown that the pH dependence is different for methane and ethane.[10,11] Koper's recent theoretical analysis of pH dependence of electrochemical reactions suggests that because ethene formation is pH-dependent on a reversible hydrogen electrode (RHE) scale that this implies the rate-determining step does not involve a proton.[12]

Recent theoretical efforts using different Kohn−Sham density functional theory (KS-DFT)-based electrochemical models have led to a variety of suggested mechanisms for C−C bond formation. A modified vacuum−surface model reported by Koper and co-workers suggests that CO dimerization occurs through surface-bound and gas-phase CO on Cu(100).[3] Using a vacuum−surface model, Nørskov and co-workers have shown that the energy barrier for CO dimerization through two adsorbed CO molecules is too large to occur at reasonable rates on Cu(211).[6] However, using a charged, explicit-water surface model, they found that CO dimerization could occur through two surface-bound CO molecules on Cu(100).[4] These authors also showed that the

Received: February 16, 2016
Accepted: April 4, 2016
Published: April 4, 2016

DOI: 10.1021/acs.jpclett.6b00358
J. Phys. Chem. Lett. 2016, 7, 1471−1477

stability of the CO dimer is strongly affected by the treatment of the surface environment; differences were observed between vacuum−surface models with and without an applied electric field and between models that include explicit water molecules at the interface (with or without charge). Very recently, Goddard and co-workers, using an approach similar to ours, found that on Cu(111) the CO dimer pathway is less favorable than the formation of an adsorbed COH followed by C−C bond formation by reaction of this species with adsorbed CO.[13] However, in a separate study using explicit water on Cu(100), this group found that the reaction to form adsorbed CHO, as opposed to COH, was preferred.[14]

Here, we present an electrochemical model for the study of C−C bond formation occurring during the electrochemical reduction of CO_2 or CO that enables us to calculate the voltage dependence of this reaction. This is a potentially important step forward because the pathway to ethene is experimentally known to be potential-dependent. Our model also includes a continuum (implicit) treatment of both the solvent and the electrolyte. We show that at low applied potential, ethene formation occurs via reaction of two surface-bound CO molecules; whereas at high applied potential, this pathway is blocked by a high barrier, and the pathway to ethene proceeds through the reaction of adsorbed CHO and CO. DFT-calculated free-energy barriers were used in a simple microkinetic model of C−C bond formation. The predictions of this model were found to agree very well with experimental current−voltage data for ethene formation.

Several groups have recently developed DFT-based electrochemical models that include the effects of solvent and electrolyte implicitly.[15−20] Here, we use the solvation program VASPsol in which the solvent is treated as a continuum dielectric.[16,21] The electrolyte is included using a linearized Poisson−Boltzmann model.[17] The methodology for handling the effects of the solvent and the electrolyte is presented in ref 17, and additional details concerning its implementation can be found there. The potential field, $\phi(\mathbf{r})$, is determined by self-consistently solving the Poisson−Boltzmann equation along with the traditional KS-DFT equations solved with inclusion of the space charge field. The linearized Poisson−Boltzmann equation is given by

$$\epsilon_b \nabla^2 \phi(\mathbf{r}) - \epsilon_b k_b^2 \phi(\mathbf{r}) = 4\pi(\rho_{DFT}(\mathbf{r}) + \rho_{ext}(\mathbf{r})) \quad (1)$$

where ϵ_b is the dielectric constant of bulk water, ρ_{DFT} the charge density of the KS-DFT system, ρ_{ext} the charge density of the bound charge and the ionic charges of the electrolyte cations and anions, and $k_b^2 = \frac{e^2}{\epsilon_b k_B T} \sum_i N_i Z_i^2$ the square of the inverse Debye screening length in the bulk electrolyte. Here, Z_i, $N_i = c_i N_A$, k_B, and T are the valence numbers, the number densities of the ionic species i in the bulk, Boltzmann constant, and temperature, respectively.

The electrode potential on the standard hydrogen electrode (SHE) scale is calculated from the Fermi energy[15] as

$$U = \frac{-\epsilon_F - \phi_{SHE}}{e} \quad (2)$$

where ϵ_F is the Fermi energy and ϕ_{SHE} is the thermodynamic work function of the SHE. We use the theoretically predicted value of ϕ_{SHE} = 4.43 eV for the RPBE functional.[22] We note that the sign convention for the work function used in eq 2 is the opposite of that used in ref 15. In accordance with convention, the Fermi energy is equal to the chemical potential for electrons. Therefore, by placing the KS-DFT system in contact with a bath of electrons at a fixed chemical potential, the number of electrons will flow to achieve equilibrium. In practice, this involves simply solving for the (fractional) number of electrons in the KS-DFT system that sets the Fermi energy such that eq 2 is equal to the desired potential. The Poisson−Boltzmann model provides charge compensation for the excess electrons required to set the desired potential; therefore, the overall simulation cell is charge-neutral and provides an absolute zero potential reference deep in the solvent region. Therefore, the Fermi energy is the energy of an electron in the electrode compared to a solvated electron; however, the solvated electron has zero energy relative to vacuum because the Poisson−Boltzmann model considers only electrostatic effects and the electrostatic potential in this region is zero. Thus, in this model, the Fermi energy is the energy of an electron in the electrode compared to vacuum.

Chart 1 shows the flowchart for our fixed-potential KS-DFT algorithm. The innermost loop, which determines the space charge field, is computed very rapidly leading to a near-negligible increase in the overall computational cost. The outermost loop, which optimizes the number of electrons to set the electrode potential, contributes the largest increase in computational cost because it requires multiple KS-DFT calculations. However, the KS-DFT orbitals from the previous iterations provide an excellent guess for the next iteration; therefore, the majority of computational cost goes into the first KS-DFT self-consistent field calculation. A simple steepest descent algorithm was used in which $d\epsilon_F/dN_e$ (where N_e is the number of electrons in the DFT system) is approximated from the previous two iterations. This scheme typically converged in fewer than 10 iterations at approximately three times the computational cost of a potential-free KS-DFT calculation. With more sophisticated convergence schemes the computa-

Chart 1. Flowchart for the Fixed Electrode Potential Self-Consistent Field Procedure[a]

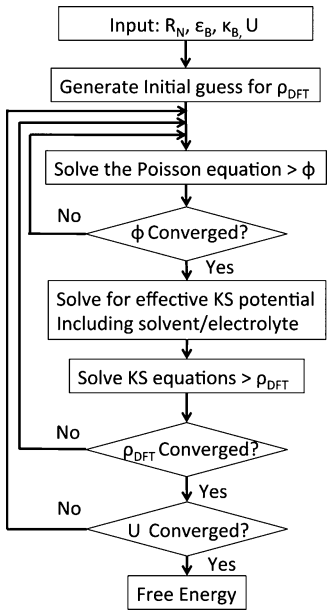

[a] R_N are the nuclear coordinates; ϵ_b is the dielectric constant of the solution, κ_b the debye screening length, and U the applied potential.

DOI: 10.1021/acs.jpclett.6b00358
J. Phys. Chem. Lett. 2016, 7, 1471−1477

tional overhead associated with the applied potential could probably be reduced further.

A chemical reaction modeled at constant bias is an open system for electrons and electrolyte ions; therefore, the change in number of these species must be included when calculating free-energy changes. The free-energy change for a process A → B is

$$\Delta G_{A\to B} = \mu^B - \mu^A - \mu_e(N_e^B - N_e^A) - \mu_+(N_+^B - N_+^A) - \mu_-(N_-^B - N_-^A) \quad (3)$$

where μ_e is the chemical potential of the electrons (the Fermi energy) and μ_+ and μ_- are the chemical potential of the cations and anions calculated as $\mu_{\mp} = k_B T \ln \frac{c_b a^3}{1 - 2c_b a^3}$, where c_b is the bulk concentration and a is the ion radius; N_e^A, N_+^A, and N_-^A are the number of electrons, total charge of cations, and total charge of anions, respectively. The total charge of cations and anions is calculated by integrating the electrolyte charge distribution $N_+^A = \int \rho_+(\mathbf{r})\, d(\mathbf{r})$. The chemical potentials for the system μ^A and μ^B are calculated using standard DFT techniques as described in the Supporting Information.

To validate the Poisson−Boltzmann model for calculation of electrochemical potentials, we determined the potential of zero charge (PZC) for several surfaces of copper, silver, nickel, and gold. Figure 1 shows excellent agreement of our RBPE-based

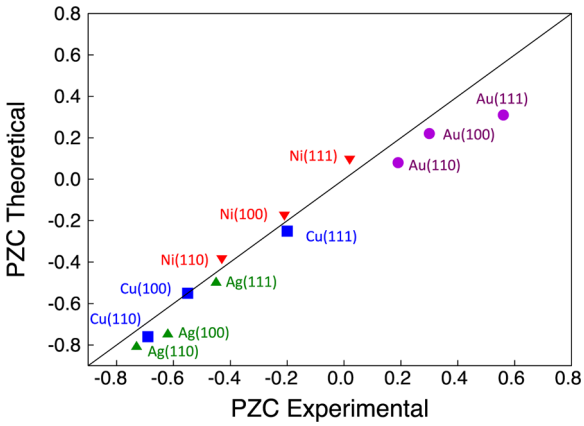

Figure 1. Comparison of the calculated and experimental potential of zero charge (PZC) on the SHE scale for various surfaces (silver, gold, nickel, and copper). The average error is 0.09 V.[26]

model with experimental results with an average error of 0.09 V, consistent with previously calculated values of PZCs using PBE.[17] As discussed previously, this model does not allow for explicit anion adsorption. Thus, the experimental PZC values used in this comparison were measured in potassium perchlorate for copper and nickel and sodium fluoride for silver and gold because these electrolytes are expected to have little to no direct adsorption.[23,24] Because CO_2 reduction is performed at significantly more negative potentials where anion adsorption would be expected to be nonexistent, we expect our model to be accurate regardless of the electrolyte used; therefore, we do not include explicit ions for any of the calculations reported here. Additionally, previous DFT calculations have shown that the equilibrium potential for the discharge and adsorption of alkali metal cations on a variety of metal surfaces occurs at potentials more negative than those considered in this study.[25] Therefore, our model accurately reproduces experimental results for a variety of metals in which the experimental measurement was performed in electrolyte with little direct absorption to the metal.

Having validated the model, we used it to identify the lowest free-energy pathways for C−C bond formation on Cu(100). Because the experimental studies have shown that the distribution of products formed via electrochemical reduction of CO_2 are the same as those formed via the reduction of CO,[11,27] we investigated the pathways by which C−C bonds could be formed starting from CO. Figure 2a shows the relative

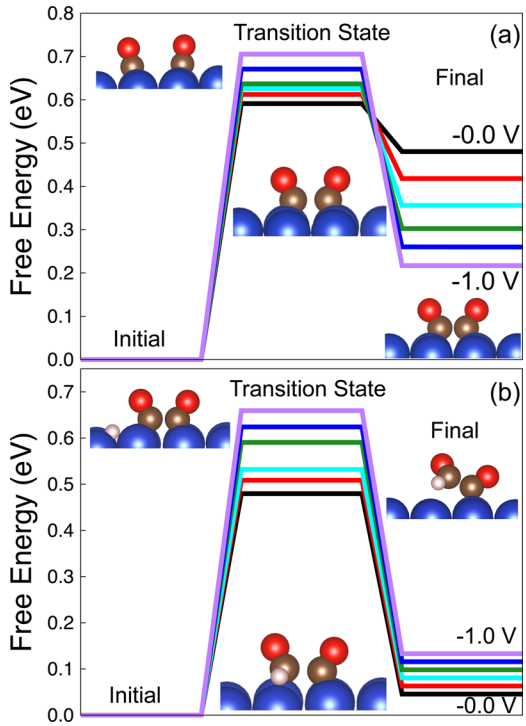

Figure 2. Relative free energy of the initial configuration, transition state, and final configuration for (a) formation of CO dimer and (b) formation of $OCCHO_{ads}$ as predicted from our electrochemical model for −1.0 V (purple), −0.8 V (blue), −0.6 V (green), −0.4 V (cyan), −0.2 V (red), and 0.0 V (black). All potentials are given versus RHE at pH 7.

free energy for CO dimerization on Cu(100). The free-energy barrier is low enough for the reaction to proceed at room temperature but increases in magnitude with increasing applied potential. The reason for this trend is that increasing the applied potential stabilizes adsorbed CO and CO dimer; CO is stabilized by increasing the electron density transferred to the $2\pi^*$ orbital, and because the dimer is more stable in its anionic form, increasing electron density on the CO dimer stabilizes this species. However, the energy required to bring two CO molecules together with larger dipoles increases with increasing applied potential, which in turn increases the free-energy barrier for the reaction.

To determine if the CO dimer is a viable intermediate on the pathway to C_2 product formation on Cu(100), we investigated how readily the CO dimer could react with hydrogen. Figure 2b shows the relative free energy for hydrogenation of the CO dimer. We note again that the free-energy barrier is low enough for the reaction to proceed at room temperature but increases in magnitude with increasing potential. This suggests that the

DOI: 10.1021/acs.jpclett.6b00358
J. Phys. Chem. Lett. 2016, 7, 1471−1477

CO dimer pathway to C_2 products will shut down at higher applied potentials because free-energy barriers for formation of the CO dimer and hydrogenation of this species, both of which must occur in order to form ethene, increase with applied potential.

To explore alternative pathways for C−C bond formation, we first determined possible surface intermediates that could form C−C bonds. We investigated the reaction of adsorbed CO to form CHO_{ads}. In the Supporting Information we show that adsorbed hydrogen can be formed on Cu(100) via a surface reduction of water in a Volmer step. Therefore, CHO_{ads} can be formed via reaction with adsorbed H, a Tafel process

$$CO_{ads} + H_{ads} \rightarrow CHO_{ads}$$

or directly from solution via reduction of water

$$CO_{ads} + H_2O_{aq} + e^- \rightarrow CHO_{ads} + OH^-_{(aq)}$$

a Heyrovsky reaction. The use of periodic boundary conditions requires that the net charge of the periodic cell be neutral; therefore, Heyrovsky reactions have been difficult to study using vacuum−surface models because there is an addition of an electron, which creates a negatively charged cell. Because our model has charge-compensating electrolytes, we are able to investigate this type of step, which is a powerful advantage of our model. In the calculations of H_{ads} and CHO_{ads}, we included one or two explicit water molecules; the number of explicit waters included for each reaction is provided in Table S1 of the Supporting Information.

Figure 3a,b compare the reaction barrier to form CHO_{ads} via the Tafel and Heyrovsky mechanisms. At all potentials, the free-energy barrier for the Tafel process remains relatively high; however, for the Heyrovsky pathway, the barrier decreases with increasing applied potential, making the reaction quite favorable at room temperature. To explore the role of water molecules in the Heyrovsky mechanism, two additional water molecules were included in the calculations. Inclusion of two water molecules increases the free-energy difference between reactant and product states by only 0.09 eV. Therefore, the inclusion of additional explicit water molecules would not significantly affect the free-energy changes reported here. A further discussion of how accurately the Poisson−Boltzmann model solvates the hydroxide anion in our electrochemical cell is given on page 5 of the Supporting Information. As shown in Figure 3b, the proton is shuttled to CO_{ads} through the closest water molecule. We also examined the possibility of a water-shuttled Volmer mechanism, but we found a free-energy barrier that was higher than that for direct hydrogenation. Because there is a viable pathway to CHO_{ads}, we next examined C−C bond formation via reaction of CHO_{ads} with CO_{ads}. Figure 3c shows the free-energy change for this reaction to be approximately the same as that for the formation of a CO dimer, but with a significantly lower potential dependence.

Additional pathways for C−C coupling were explored, but all cases resulted in free energies of activation that were higher than those for the two processes considered above. Of particular note, the free energy of activation for C−C bond formation via reaction of two CHO_{ads} species was found to be 0.15 eV higher than that for the reaction of CHO_{ads} and CO_{ads}. In agreement with previous results,[28] we found reaction of CO_{ads} with hydrogen to form COH_{ads} to have a barrier of 1.03 eV. However, in contrast to the earlier reported study, we did not observe the free energy of activation to decrease significantly with applied potential. Therefore, we find

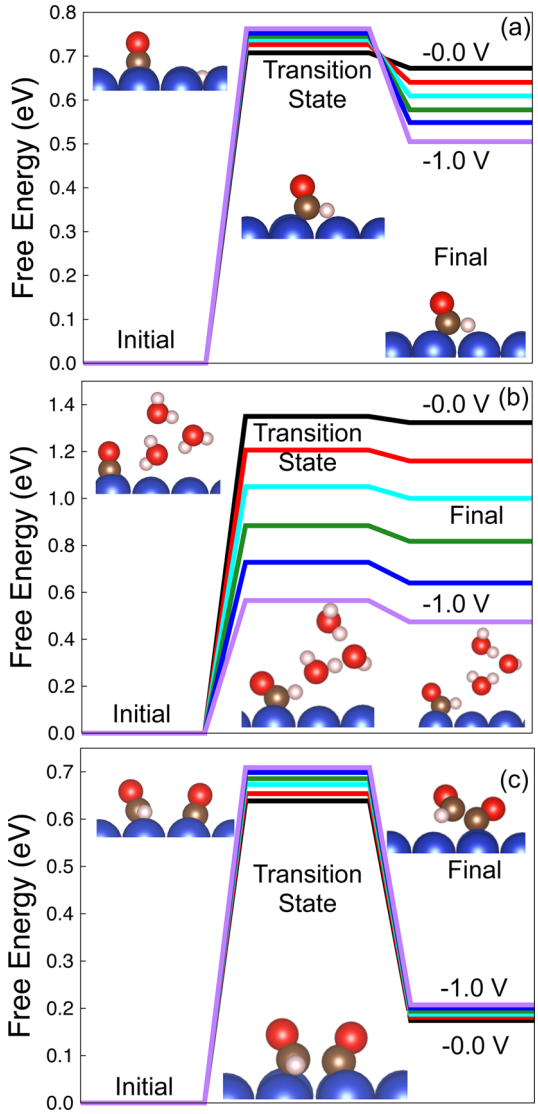

Figure 3. Relative free energy of the initial configuration, transition state, and final configuration for (a) formation of CHO_{ads} through a Volmer mechanism, (b) formation of CHO_{ads} through a Heyrovsky mechanism, and (c) formation of $CHOCO_{ads}$ predicted from our electrochemical model for −1.0 V (purple), −0.8 V (blue), −0.6 V (green), −0.4 V (cyan), −0.2 V (red), and 0.0 V (black). All potentials are given versus RHE at pH 7.

formation of COH_{ads} to be an unlikely step in C−C bond formation (i.e., reaction of COH_{ads} and CO_{ads}) at room temperature. Instead, we believe that COH_{ads} will undergo hydrogenation to form $HCOH_{ads}$, an intermediate that would proceed rapidly to methane.[14]

As stated earlier, the model used in the present study is similar to the JDFT model used by Goddard and co-workers.[13] We note, though, that our model includes the free-energy change due to the change in the number of ions, following the work of Anderson and Jinnouchi.[15] Although for the majority of the reactions this term is small, for the Heyrovsky pathways this term can be larger than 0.2 eV. Additionally, while including pH as a constant shift is certainly appealing, as we will show below, CO (and thus CO_2) reduction is a very complicated reaction, and more sophisticated methods will be required to fully understand the effect of pH on CO_2 reduction.

DOI: 10.1021/acs.jpclett.6b00358
J. Phys. Chem. Lett. 2016, 7, 1471−1477

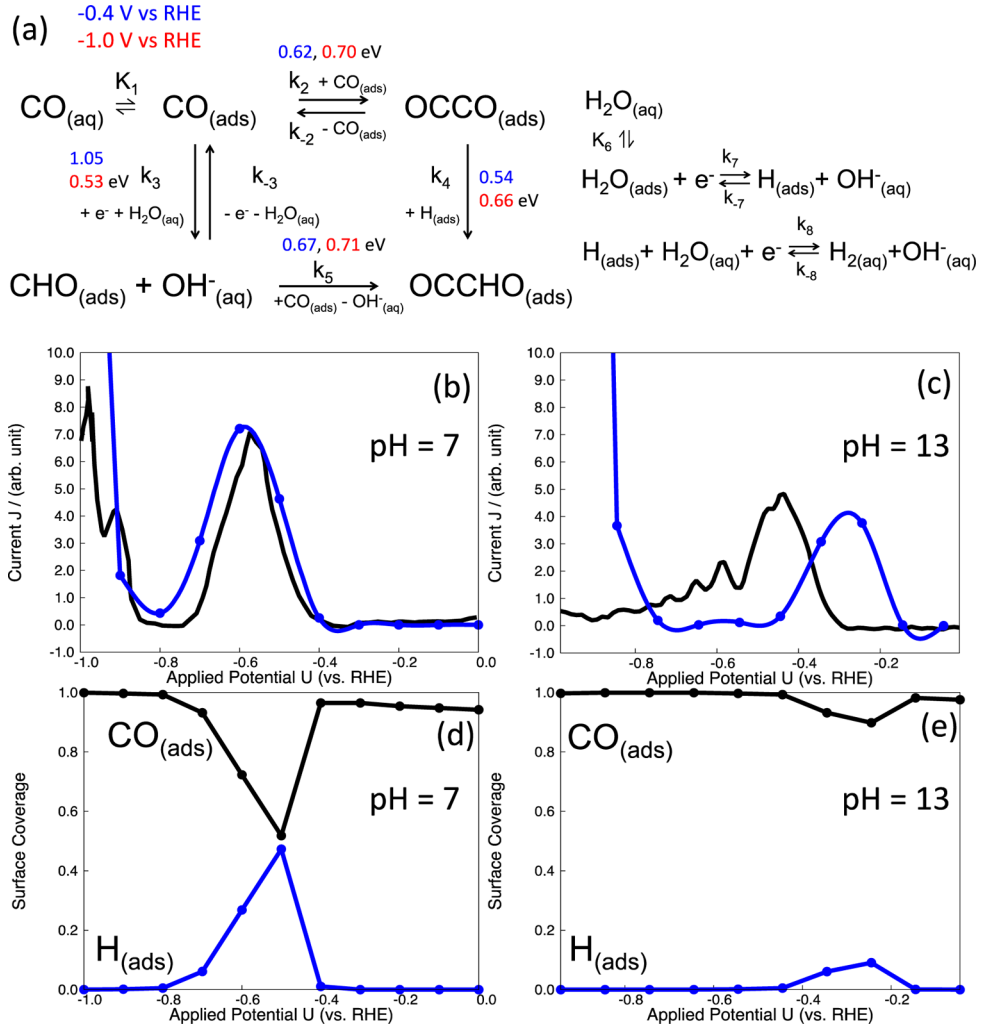

Figure 4. (a) Reactions considered in the microkinetic model for C−C bond formation with the forward barrier heights for different applied potentials given versus RHE at pH 7. (b,c) The negative scan of a cyclic voltammogram for the reduction of CO contained in a CO-saturated solution of 0.1 M K_2HPO_4 and 0.1 M KH_2PO_4 at pH 7 (b) or 0.1 M NaOH at pH 13 (c) on Cu(100). The experimental results are shown in black, and the results obtained from the microkinetic model are shown in blue. (d,e) The surface coverage for CO (black) and H (blue) for pH 7 (d) and for pH 13 (e).

Figure 4a illustrates the effects of applied potential on the free energies of activation at −0.4 and −1.0 V versus RHE. It is clear that at −0.4 V, C−C bond formation via a CO dimer is preferred, but at −1.0 V, C−C bond formation occurs preferentially via CO_{ads} and CHO_{ads}. To further support the hypothesis, we developed a microkinetic model to describe the kinetics of C−C bond formation. Our model includes the reactions shown in Figure 4a and assumes that adsorbed CO and water are equilibrated with the aqueous phase. This model further assumes that if $OCCHO_{ads}$ is formed, these intermediates undergo rapid hydrogenation to produce ethene. This assumption is supported by Figure S2, which shows that the free energy of activation for the hydrogenation of $OCCHO_{ads}$ to form $OCCHOH_{ads}$ is relatively low (0.45−0.55 eV).

The free-energy barriers can be used with transition-state theory to calculate potential-dependent rate constants. The rate of the nth reaction is

$$k_n = \frac{k_B T}{h} \exp[-\Delta G^{\dagger}(U)/k_B T] \tag{4}$$

where $\Delta G^{\dagger}(U)$ is the potential-dependent free-energy barrier calculated from our model. The surface reaction rate for the nth reaction is

$$-r_n = k_n \theta_n \tag{5}$$

where r_n is the rate of reaction, k_n the elementary rate constant, and θ_n the surface fraction of the species. Equations 4 and 5 can then be used to calculate the partial current density to ethene as

$$J = 8eA\left(\frac{k_4\theta_{CO}\theta_{CHO}}{S_{CO}S_{CHO}} + \frac{k_5\theta_H\theta_{OCCO}}{S_H S_{OCCO}}\right) \tag{6}$$

where 8 is the number of electrons required to reduce two CO molecules to ethene, e the charge on an electron, and A the number of surface atoms per area; S_{CO}, S_{CHO}, S_H, and S_{OCCO} are the number of sites per adsorbed surface molecules which were set to 1, 1, 1, and 2, respectively.[29] Additional details of the microkinetic model are provided in the Supporting Information.

The blue curve in Figure 4b illustrates the partial current for the formation of C−C bond containing intermediates determined from our microkinetic model. These are the

DOI: 10.1021/acs.jpclett.6b00358
J. Phys. Chem. Lett. 2016, 7, 1471−1477

species which then undergo further hydrogenation to form ethene. The black curve in this figure illustrates the experimental results for ethene formation reported by Koper and co-workers.[8] The agreement between theory and experiment is very good at pH 7, suggesting that our two-pathway mechanism provides a plausible explanation for the experimental results. Figure 4c shows the surface coverages of H_{ads} and CO_{ads} as functions of potential. At low applied potential, CO_{ads} dominates the surface. As the onset of CO reduction occurs, hydrogen evolution competes for the open sites, increasing the fraction of the surface covered by H_{ads}. However, at high applied potential, the coverage of H_{ads} decreases again as the barrier to form H_2 decreases and significant hydrogen is evolved. The coverage by CHO_{ads} and CO dimers remains very low for all potentials ($\sim 10^{-4}$). Our findings suggest that it will be extremely challenging to detect adsorbed intermediates involved in the formation of hydrocarbons and that the only species readily detectable would be CO_{ads} and H_{ads}.

If the reaction mechanism for C−C formation is taken to be pH-independent, one would expect the pH change from 7 to 13 to lead to constant shift of 59.2 mV/pH, or 0.355 V. In our microkinetic model, the pH enters not only in the constant shift but also in the formation rates of CHO_{ads} and H_{ads}. The blue curve in Figure 4c shows how a change from pH 7 to pH 13 affects the partial current density to ethene. Impressively, our model recovers the correct relative current density for the first peak. Our microkinetic model shows a peak shift of 0.30 V, and while that is quantitatively incorrect as experimentally the shift is only 0.2 V, it is qualitatively smaller than the constant shift of 0.355 V. Additionally, at large negative potentials, the experimentally observed current density is near zero for ethene, whereas our model, similar to pH 7, shows a rise in current density. The small current at large negative potential is from the fact that the pathway to form CHO_{ads} is completely blocked at pH 13; however, our model suggests that at large enough overpotential the pathway to form CHO_{ads} will reopen. The model's prediction that the pathway to form CHO_{ads} will be fast in the large overpotential region is perhaps due to the linearized Poisson−Boltzmann model breaking down at high overpotentials or that in this region the electron transfer is not adiabatic, causing a slowing of the reaction rate. Therefore, given the qualitative agreement with experiment at both pH 7 and 13, our simple microkinetic model suggests that the two pathways proposed for C−C bond formation are able to explain the experimental data.

In conclusion, we have developed a model for predicting the Gibbs free energy of activation of elementary steps involved in the electrochemical reduction of CO_2. This model represents the electrolyte as a continuum dielectric and uses the linearized Poisson−Boltzmann equation to determine the space-charge field imposed by the electrolyte on the species adsorbed on the electrode surface. The effects of the space-charge field are then included in DFT calculations of the energies and free energies. We have applied this model to the elementary reaction steps involved in the electrochemical reduction of CO_2 (CO) on the surface of Cu(100). Our results suggest that the mechanism by which C−C bonds are formed depends on the applied potential. At low overpotentials, C−C bond formation proceeds via formation of a CO dimer, whereas at high overpotentials, C−C bond formation occurs via reaction of CO_{ads} and CHO_{ads}.

■ ASSOCIATED CONTENT

Supporting Information

The Supporting Information is available free of charge on the ACS Publications website at DOI: 10.1021/acs.jpclett.6b00358.

Calculation parameters and details on thermodynamic and kinetic data along with the working equations for the microkinetic model (PDF)

■ AUTHOR INFORMATION

Corresponding Authors

*E-mail: alexbell@berkeley.edu.

*E-mail: mhg@cchem.berkeley.edu.

Notes

The authors declare no competing financial interest.

■ ACKNOWLEDGMENTS

This material is based on work performed in the Joint Center for Artificial Photosynthesis, a DOE Energy Innovation Hub, supported through the Office of Science of the U.S. Department of Energy under Award DE-SC00004993. The authors thank Richard Hennig for providing the linearized Poisson−Boltzmann code for VASP and the VASPsol program.

■ REFERENCES

(1) Beer, C.; Reichstein, M.; Tomelleri, E.; Ciais, P.; Jung, M.; Carvalhais, N.; Rödenbeck, C.; Arain, M. A.; Baldocchi, D.; Bonan, G. B.; Bondeau, A.; Cescatti, A.; Lasslop, G.; Lindroth, A.; Lomas, M.; Luyssaert, S.; Margolis, H.; Oleson, K. W.; Roupsard, O.; Veenendaal, E.; Viovy, N.; Williams, C.; Woodward, F. I.; Papale, D. Terrestrial Gross Carbon Dioxide Uptake: Global Distribution and Covariation with Climate. *Science* **2010**, *329* (5993), 834−838.

(2) Kortlever, R.; Shen, J.; Schouten, K. J. P.; Calle-Vallejo, F.; Koper, M. T. M. Catalysts and Reaction Pathways for the Electrochemical Reduction of Carbon Dioxide. *J. Phys. Chem. Lett.* **2015**, *6* (20), 4073−4082.

(3) Calle-Vallejo, F.; Koper, M. T. Theoretical considerations on the electroreduction of CO to C_2 species on Cu(100) electrodes. *Angew. Chem., Int. Ed.* **2013**, *52* (28), 7282−5.

(4) Montoya, J. H.; Shi, C.; Chan, K.; Norskov, J. K. Theoretical Insights into a CO Dimerization Mechanism in CO_2 Electroreduction. *J. Phys. Chem. Lett.* **2015**, *6* (11), 2032−7.

(5) Ou, L.; Long, W.; Chen, Y.; Jin, J. *RSC Adv.* **2015**, *5*, 96281−96289.

(6) Montoya, J. H.; Peterson, A. A.; Nørskov, J. K. Insights into C-C Coupling in CO2Electroreduction on Copper Electrodes. *ChemCatChem* **2013**, *5* (3), 737−742.

(7) Schouten, K. J. P.; Gallent, E. P.; Koper, M. T. M. The electrochemical characterization of copper single-crystal electrodes in alkaline media. *J. Electroanal. Chem.* **2013**, *699*, 6−9.

(8) Schouten, K. J.; Qin, Z.; Gallent, E. P.; Koper, M. T. Two pathways for the formation of ethylene in CO reduction on single-crystal copper electrodes. *J. Am. Chem. Soc.* **2012**, *134* (24), 9864−9867.

(9) Schouten, K. J. P.; Pérez Gallent, E.; Koper, M. T. M. Structure Sensitivity of the Electrochemical Reduction of Carbon Monoxide on Copper Single Crystals. *ACS Catal.* **2013**, *3* (6), 1292−1295.

(10) Schouten, K. J. P.; Pérez Gallent, E.; Koper, M. T. M. The influence of pH on the reduction of CO and to hydrocarbons on copper electrodes. *J. Electroanal. Chem.* **2014**, *716*, 53−57.

(11) Hori, Y. Electrochemical CO_2 Reduction on Metal Electrodes. In *Modern Aspects of Electrochemistry*,; Vayenas, C., White, R., Gamboa-Aldeco, M., Eds.; Springer: New York, 2008; Vol. *42*, pp 89−189.

(12) Koper, M. T. M. Theory of multiple proton−electron transfer reactions and its implications for electrocatalysis. *Chemical Science* **2013**, *4* (7), 2710.

DOI: 10.1021/acs.jpclett.6b00358
J. Phys. Chem. Lett. 2016, 7, 1471−1477

(13) Xiao, H.; Cheng, T.; Goddard, W. A., III; Sundararaman, R. Mechanistic Explanation of the pH Dependence and Onset Potentials for Hydrocarbon Products from Electrochemical Reduction of CO on Cu (111). *J. Am. Chem. Soc.* **2016**, *138* (2), 483−6.
(14) Cheng, T.; Xiao, H.; Goddard, W. A., III. Free-Energy Barriers and Reaction Mechanisms for the Electrochemical Reduction of CO on the Cu(100) Surface, Including Multiple Layers of Explicit Solvent at pH 0. *J. Phys. Chem. Lett.* **2015**, *6*, 4767−4773.
(15) Jinnouchi, R.; Anderson, A. B. Electronic structure calculations of liquid-solid interfaces: Combination of density functional theory and modified Poisson-Boltzmann theory. *Phys. Rev. B: Condens. Matter Mater. Phys.* **2008**, *77* (24). DOI: 10.1103/PhysRevB.77.245417
(16) Mathew, K.; Sundararaman, R.; Letchworth-Weaver, K.; Arias, T. A.; Hennig, R. G. Implicit solvation model for density-functional study of nanocrystal surfaces and reaction pathways. *J. Chem. Phys.* **2014**, *140* (8), 084106.
(17) Letchworth-Weaver, K.; Arias, T. A. Joint density functional theory of the electrode-electrolyte interface: Application to fixed electrode potentials, interfacial capacitances, and potentials of zero charge. *Phys. Rev. B: Condens. Matter Mater. Phys.* **2012**, *86* (7). DOI: 10.1103/PhysRevB.86.075140
(18) Petrosyan, S. A.; Briere, J.-F.; Roundy, D.; Arias, T. A. Joint density-functional theory for electronic structure of solvated systems. *Phys. Rev. B: Condens. Matter Mater. Phys.* **2007**, *75* (20). DOI: 10.1103/PhysRevB.75.205105
(19) Gunceler, D.; Letchworth-Weaver, K.; Sundararaman, R.; Schwarz, K. A.; Arias, T. A. The importance of nonlinear fluid response in joint density-functional theory studies of battery systems. *Modell. Simul. Mater. Sci. Eng.* **2013**, *21* (7), 074005.
(20) Fishman, M.; Zhuang, H. L.; Mathew, K.; Dirschka, W.; Hennig, R. G. Accuracy of exchange-correlation functionals and effect of solvation on the surface energy of copper. *Phys. Rev. B: Condens. Matter Mater. Phys.* **2013**, *87* (24). DOI: 10.1103/PhysRevB.87.245402
(21) Fishman, M.; Zhuang, H. L.; Mathew, K.; Dirschka, W.; Hennig, R. G. Accuracy of exchange-correlation functionals and effect of solvation on the surface energy of copper. *Phys. Rev. B: Condens. Matter Mater. Phys.* **2013**, *87* (24), 245402.
(22) Jinnouchi, R.; Anderson, A. B. Aqueous and Surface Redox Potentials from Self-Consistently Determined Gibbs Energies. *J. Phys. Chem. C* **2008**, *112* (24), 8747−8750.
(23) Koga, O.; Watanabe, Y.; Tanizaki, M.; Hori, Y. Specific adsorption of anions on a copper (100) single crystal electrode studied by charge displacement by CO adsorption and infrared spectroscopy. *Electrochim. Acta* **2001**, *46* (20−21), 3083−3090.
(24) Bacchetta, M.; Trasatti, S.; Doubova, L.; Hamelin, A. Specific adsorption of fluoride ions on the (110) face of a silver single crystal electrode. *J. Electroanal. Chem. Interfacial Electrochem.* **1988**, *255* (1−2), 237−249.
(25) Mills, J. N.; McCrum, I. T.; Janik, M. J. Alkali cation specific adsorption onto fcc(111) transition metal electrodes. *Phys. Chem. Chem. Phys.* **2014**, *16* (27), 13699−707.
(26) *Modern Aspects of Electrochemistry*; Springer US: New York, 1999; p 644.
(27) Hori, Y.; Kikuchi, K.; Suzuki, S. Production of CO and CH_4 in electrochemical reduction of CO_2 at Metal Electrodues in Aqeous Hydrogencarbonate Solution. *Chem. Lett.* **1985**, *14* (11), 1695−1698.
(28) Nie, X.; Esopi, M. R.; Janik, M. J.; Asthagiri, A. Selectivity of CO_2 reduction on copper electrodes: the role of the kinetics of elementary steps. *Angew. Chem., Int. Ed.* **2013**, *52* (9), 2459−62.
(29) Rostamikia, G.; Mendoza, A. J.; Hickner, M. A.; Janik, M. J. First-principles based microkinetic modeling of borohydride oxidation on a Au(111) electrode. *J. Power Sources* **2011**, *196* (22), 9228−9237.

DOI: 10.1021/acs.jpclett.6b00358
J. Phys. Chem. Lett. 2016, 7, 1471−1477